

On the role of the imide axial ligand in the spin and
oxidation state of Mn corrole and corrolazine
complexes

Gerard Alcover-Fortuny,^a Rosa Caballol,^a Kristine Pierloot,^b Coen de Graaf^{a,c}

(a) Departament de Química Física i Inorgànica, Universitat
Rovira i Virgili, Marcel·lí Domingo s/n, 43007 Tarragona, Spain

(b) Department of Chemistry, University of Leuven,
Celestijnenlaan 200F, B-3001 Heverlee-Leuven, Belgium

(c) Institutació Catalana de Recerca i Estudis Avançats (ICREA)
Passeig Lluis Companys 23, 08010, Barcelona, Spain

March 1, 2016

Abstract

Electronic structure calculations have been performed on four different Mn corrole and corrolazine complexes to clarify the role of the imide axial ligand on the relative stability of the different spin states and the stabilization of the high valent Mn ion in these complexes. Multiconfigurational perturbation theory energy calculations on the DFT optimized geometries shows that all complexes have a singlet ground state except the complex with the strongest electron withdrawal axial ligand, which is found to have a triplet ground state. The analysis of the sigma and pi interaction between metal and imide ligand shows that this spin crossover is caused by a subtle interplay of geometrical factors (Mn-N distance and coordination angle) and the electron withdrawal character of the imide. The analysis of the multiconfigurational wave functions reveals that the formally Mn^V ion is stabilized by an important electron transfer from both the equatorial corrole/corrolazine ligand and the axial imide. The macrocycle donates roughly half an electron, being somewhere between the closed-shell trianionic and the dianionic radical form. The imide ligand transfers 2.5 electrons to the metal center, resulting in an effective d-electron count close to five in all complexes.

1 Introduction

The planar structure of transition metal (TM) porphyrins and their derivatives favours binding of axial ligands to the metal centre and is a key factor in many biological processes. Axial ligands often directly affect the magnetic properties and the reactivity of these compounds. A well-known example is haemoglobin containing a high-spin ferrous porphyrin active site which becomes low-spin when an O₂ molecule axially coordinates to the TM. However, attempts to completely understand the mechanism of these reactions are sometimes frustrated by the fast kinetics and the thermodynamic instability of the intermediates. This is the case of the Cytochrome P450 family of enzymes, responsible for many reactions involving biodegradation and biosynthesis. The activated intermediate of such reactions, known as Compound I, consists of a high-valent Fe-porphyrin with an oxygen atom axially coordinated, which is transferred to the organic substrate [1–6].

The interest in enzymatic processes lies, among other reasons, in the fact that such reactions have motivated the design of model systems with applications as synthetic catalysts. For instance, many biomimetic compounds inspired by Cytochrome P450 have been developed since the early 1980s to catalyze group transfer reactions [7–14]. With direct influence on the kinetics of these reactions, the energetics of the low-lying spin states in these TM-porphyrins deserves special attention. In organometallic chemistry, some reactions involve spin state crossings in what is termed "two-state reactivity" [15] resulting sometimes in a slowdown of the kinetics, known as spin crossing effect [16, 17]. Unusual kinetic stability for oxo-Mn^V porphyrin complexes was reported as an example of this spin crossing effect, since the rate of the Mn^V reduction is significantly slower than for its Mn^{IV} analogue. Reduction of the low-spin (S=0) Mn^V complex with a closed-shell d² electronic configuration (Fig.1, centre right) to a d³ Mn^{IV} implies not only the addition of one electron but also the promotion of an electron from 3d_{xy} to 3d_{xz} or 3d_{yz} and the consequent change to a high-spin (S=3/2) configuration (Fig.1 centre left). This change in the spin state adds a kinetic barrier to the reaction path which is nonexistent in the reduction of the Mn^{IV} analogue [18–20]. Changes in the axial ligand can stabilize the Mn^V 3d_{xz,yz} orbitals favouring the high-spin (S=1) state (Fig.1 right) and facilitating the reduction to Mn^{IV}.

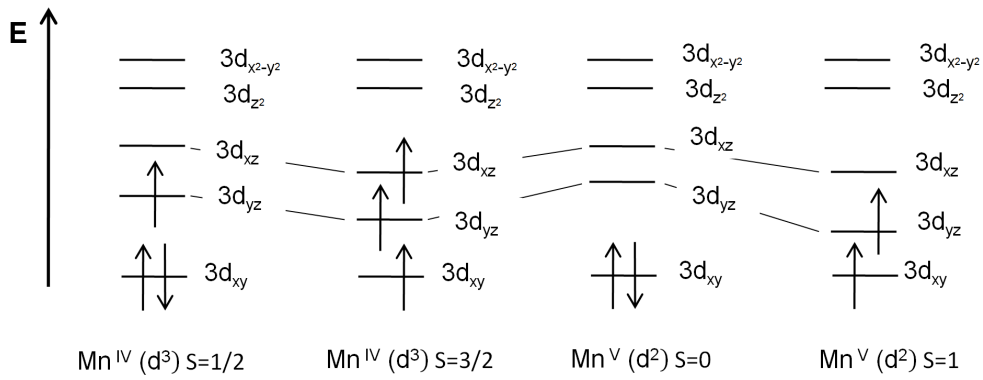


Figure 1: Low- ($S=1/2$) and high-spin ($S=3/2$) Mn^{IV} (*left*) and low- ($S=0$) and high-spin ($S=1$) Mn^V (*right*) spin configurations of the Mn ion in the quasi-square pyramid coordination sphere of the oxo-Mn(porphyrin) system with the nitrogens of the pyrrole rings placed on the x - and y -axes.

This example shows how porphyrin stabilizes transition metal ions with unusually high oxidation states [21], but corrole (Cor), one *meso* carbon atom shorter, has been postulated to be even more effective for this purpose. The most important difference in the corrole structural skeleton with respect to porphyrin (Fig.2) is that while the latter coordinates to the metal as a dianionic ligand, the former is trianionic [22]. Although corrole was first reported in 1964 [23], the interest in this macrocycle has increased since 1999 when simpler synthetic pathways were developed [24–26], emphasizing the large applications range of corrole and its TM complexes [27, 28]. This interest has resulted in several experimental and theoretical studies on corrole X-ray structure, spectroscopy and electronic structure [29–34].

The formal oxidation states of TMs in corrole (Cu^{III} , Ag^{III} , Fe^{IV} , Fe^V , Cr^{IV} , Cr^V , Co^V , Mn^{IV} , Mn^V) are higher than in porphyrin but the metal centre in a TM(Cor) is not necessarily high-valent and sometimes, corrole is expected to act as a dianionic radical instead of a closed-shell trianion. For example, the electronic structure of the triplet state in Mn^V corroles can be described with either a high spin ($S=1$) Mn^V (Fig.1 right) with an innocent, closed-shell trianionic corrole or with a low spin ($S=1/2$) Mn^{IV} (Fig.1 left) ferromagnetically coupled to a one-electron radical dianionic corrole acting as a non-innocent ligand [32]. Once again, the nature of the axial ligand is a crucial

factor in this non-innocent behaviour. The capability of corrole to stabilize unusual oxidation states of TM has often been attributed both to its 3- charge and to its strong σ -donor ligand field. The cavity size of the more recent corrolazine (Cz) derivative, first synthesized in 2001 [35], is smaller than in corrole, which enhances the σ -donation. In addition, the *meso*-substituted nitrogen atoms (Fig.2) are more electronegative than carbon and contribute to the electron-deficiency of the coordination sphere, favouring the 3- charge of the ligand over the dianionic radical state [36, 37]. DFT calculations on several TM(Cz) complexes have shown small spin population on the macrocyclic ligand, indicating the strong tendency of corrolazine to stabilize high oxidation states of the coordinated TM ions [38].

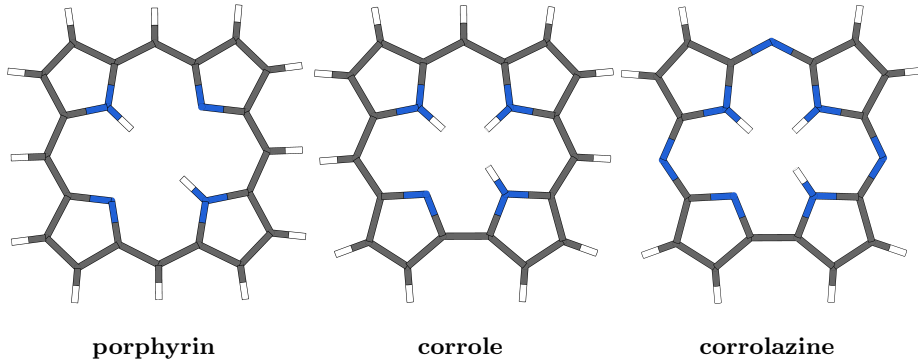


Figure 2: Porphyrin, the one *meso* carbon atom shorter derivative corrole, and its nitrogen *meso*-substituted derivative, corrolazine.

As seen above, small structural variations in the axial ligand and the macrocycle result in important changes in the spin and oxidation state of the metal centre, which directly affects the reactivity of the complex [39]. In order to catalyze oxygen transfer reactions, $Mn^V(\text{Cor})(\text{O})$ [40–43] and $Mn^V(\text{Cz})(\text{O})$ [44–46] have been synthesized. Similar to their oxo derivatives, imido- (NR) manganese corrole and corrolazine have attracted interest due to their potential applications, but not much is known about their properties. $Mn(\text{tpfc})(\text{NMes})$ (tpfc = tris(pentafluorophenyl)corrole), $Mn(\text{tpfc})(\text{NtClPh})$ [47, 48], $Mn(\text{tbpcz})(\text{NMes})$ (tbpcz = octakis(*p*-*tert*-butylphenyl)corrolazine) [49] and $Mn(\text{tpfc})(\text{NTs})$ [50] are the few examples reported. NMes, NtClPh and NTs (Fig.3) axially coordinate to the metal as dianionic ligands with distances typically assigned to

a $M\equiv N$ bond, giving rise to neutral complexes with formally high-valent Mn^V . Interestingly, while complexes with NMes and NtClPh are characterized as diamagnetic ($S=0$) by 1H and ^{19}F NMR spectroscopy, magnetic measurements on the NTs derivative give a magnetic moment associated with a paramagnetic ($S=1$) state on the Mn^V [51]. No low-lying Mn^{IV} states with a radical on corrole or corrolazine are expected since they are high-lying in the oxo derivatives [32]. The present work describes a comprehensive DFT and CASPT2 computational study on imido-Mn corrole and corrolazine complexes. It focuses on the geometrical parameters, the lowest Mn ($S=0$) and ($S=1$) spin states and the role of the three main actors (metal, macrocycle and imide) on the spin and oxidation states of $Mn(Cor)(NMes)$, $Mn(Cz)(NMes)$, $Mn(Cor)(NtClPh)$ and $Mn(Cor)(NTs)$. The main conclusion from the DFT and CASPT2 calculations is that for the NTs ligand the weak π -donation and the $Mn-N_{axial}-S$ coordination angle favour a triplet ground state. An orthogonal valence bond analysis of the electronic structure of the four complexes reveals that nearly 3 electrons (0.5 from corrole and 2.5 from the ligand) are transferred to the metal centre, stabilizing the TM ion.

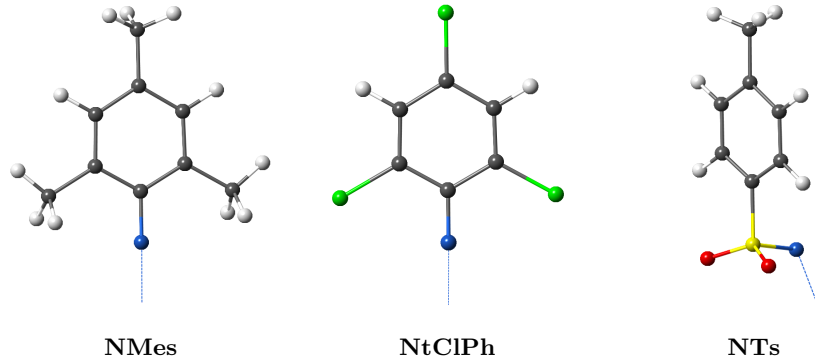


Figure 3: Axial imide ligands N-mesityl (NMes), N-(2,4,6-trichlorophenyl) (NtClPh) and N-tosyl (NTs).

2 DFT geometry optimizations

DFT geometry optimizations have been carried out for both singlet and triplet states of the four imido-complexes using def2-TZVP basis set [52, 53]. First of all, PBE0 [54–56] and B-P [57, 58] functionals have been compared on $Mn(Cor)(NMes)$. The

triplet state in the PBE0 calculation shows a considerable spin contamination ($\langle \hat{S}^2 \rangle = 3.74$) resulting in a severe overestimation of the Mn-L_{axial} bond distance. On the other hand, DFT calculations with the B-P functional do not show such anomalous spin contamination ($\langle \hat{S}^2 \rangle = 2.14$) and the optimized M-L_{axial} bond distance is 1.70 Å, much shorter than the 2.03 Å PBE0 bond length. Since the axial coordination distance is expected to play a crucial role in the relative stability of the spin-states, the B-P functional has been chosen to perform DFT geometry optimizations. To start, we have explored all possible orientations of the axial ligand for the NTs complex. Rotating the complex around the Mn-N_{axial} axis in intervals of 45°, four alternated and eclipsed conformations have been optimized with B-P/TZVP. Eclipsed conformations have the R moiety of the axial ligand aligned with N_{pyrrole}. The resulting steric repulsion lengthens the Mn–N_{axial} bond distance and closes the Mn–N_{axial}–S angle preferred by the triplet state. In contrast, as can be seen in Fig. 4, this repulsion is avoided in alternated conformations favouring singlet states with short axial distances and linear coordination angles.

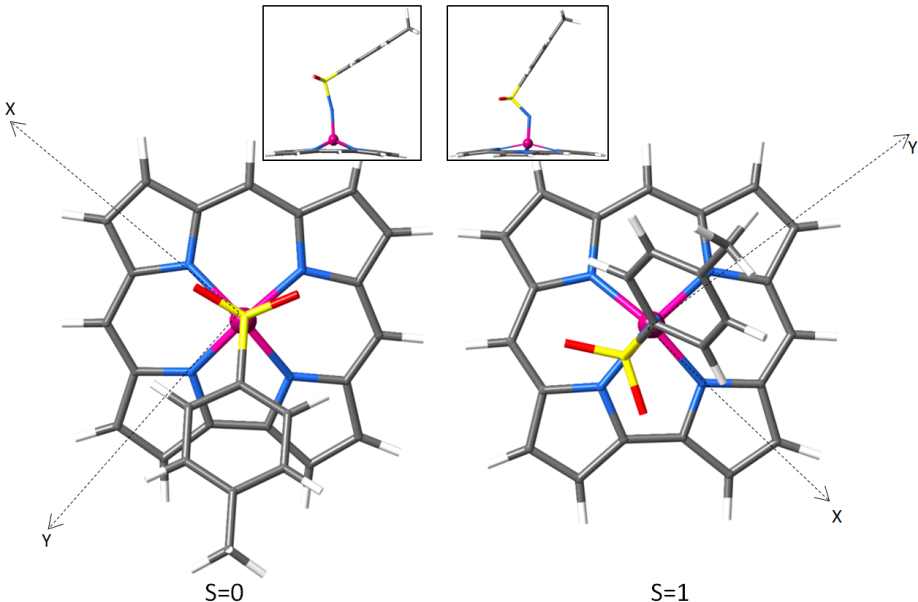


Figure 4: Most stable DFT conformations, with the R moiety between N_{pyrrole} (alternated) for the singlet and with the R moiety aligned with N_{pyrrole} (eclipsed) for the triplet.

The most important structural parameters and the relative energies of the B-P/def2-TZVP geometry optimization are summarized in Table 1. Mn(Cor)(NMes) and Mn(Cz)(NMes) results are in good agreement with the experimental X-ray structures [47, 49]. Experimental data are not available for Mn(Cor)(NtClPh) but are expected to be similar to Mn(Cor)(NMes). The structure of Mn(Cor)(NTs) has not been determined but the theoretical estimates can be compared with the X-ray structure of the chromium analogue [50]. In the low-spin state all four ligands axially bind to the Mn(Cor) and Mn(Cz) moieties in a linear fashion, forming a $\text{Mn}\equiv\text{N}$ bond, typical of imido-complexes. In all cases the Mulliken spin density in the triplet state gives almost 2.3 alpha electrons on the metal centre and 0.2 beta electrons on N_{axial} , confirming that in this state the unpaired electrons are localized on Mn. This indicates that states with a radical on corrole or corrolazine are higher in energy (see Fig. 5).

Table 1: Relevant B-P/def2-TZVP optimized geometrical parameters for the four imido-complexes. Distances and out of $N_{pyrrole}$ plane displacement (Δ) in Å, angles in degrees and relative energies in eV. Experimental values are given in parenthesis [47, 49, 50].

	Mn-N _{pyrrole}	Mn-N _{axial}	Mn-N _{axial-R}	Δ	relative energy
Mn(Cor)(NMes)					
S=0	1.92 - 1.95 (1.89 - 1.95)	1.61 (1.61)	179.2 (170.4)	0.54 (0.51)	0.00
S=1	1.93 - 1.95	1.70	145.9		0.67
Mn(Cz)(NMes)					
S=0	1.89 - 1.91 (1.87 - 1.91)	1.61 (1.61)	178.6 (176.9)	0.59 (0.55)	0.00
S=1	1.90 - 1.93	1.69	145.5		0.64
Mn(Cor)(NtClPh)					
S=0	1.91 - 1.95	1.62	179.1	0.55	0.00
S=1	1.92 - 1.95	1.70	144.1		0.52
Mn(Cor)(NTs)					
S=0	1.92 - 1.94	1.62	167.0	0.56	0.00
S=1	1.91 - 1.95 (1.92 - 1.97)	1.71 (1.65)	132.0 (150.7)		0.30

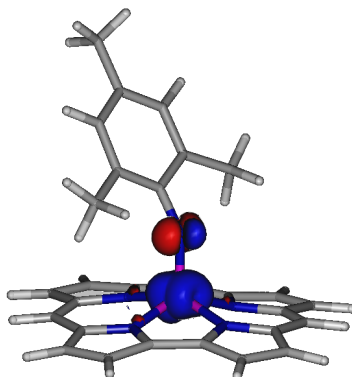


Figure 5: Spin density in the Mn(Cor)(NMes) triplet state B-P/def2-TZVP optimized geometry (isocontour=0.009).

As expected, corrolazine coordinates to Mn with shorter distances ($\text{Mn-N}_{\text{pyrrole}}$) due to the smaller cavity size, which is also responsible for a larger out of $\text{N}_{\text{pyrrole}}$ plane displacement of the metal centre (Δ). This Δ is noticeable in all complexes and induces bonding and anti-bonding mixing between the $\text{N}_{\text{pyrrole}} \sigma$ and the $3d_{xz,yz}$ orbitals (see Fig. 6). The corrole and corrolazine macrocycles show a ruffling distortion in the triplet state making it impossible to quantify Δ . The increased mixing widens the gap between the $3d_{xy}$ and the $3d_{xz,yz}$ orbitals, favouring the double occupation of the $\text{Mn-}3d_{xy}$ orbital and stabilizing the singlet state [59]. In the triplet state, the distance between Mn and the axial ligand increases due to the occupation of one of the π anti-bonding ($3d_{xz}-2p_x$)^{*} or ($3d_{yz}-2p_y$)^{*}.

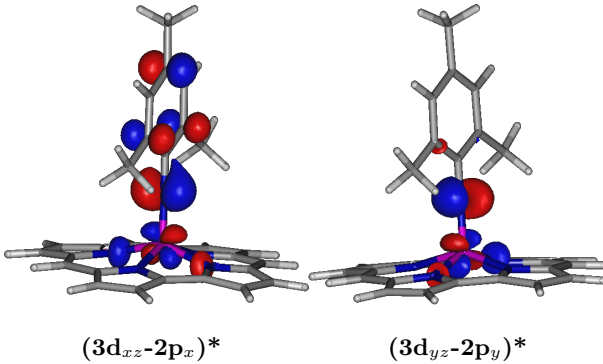


Figure 6: Anti-bonding mixing of $2p_{x,y}$ N_{axial} and σ $\text{N}_{\text{pyrrole}}$ orbitals with $3d_{xz,yz}$ of Mn (isocontour=0.05).

3 Multiconfigurational wave function calculations

DFT is known to provide suitable geometries for most TM complexes, but it is more complicated to precisely estimate the relative energies of different spin states [60–62]. In general, local density and gradient corrected functionals tend to overestimate the stability of the low-spin states. In line with this observation, we observe that the B-P calculations predict singlet ground states for all the imide derivatives. However, these results are not completely consistent with experimental data in $\text{Mn}(\text{Cor})(\text{NTs})$, which is assigned as a triplet by magnetic susceptibility measurements. Therefore, we will now proceed with the discussion of the multiconfigurational wave function description

of the electronic states, which gives, in principle, more accurate relative energies.

3.1 Single point energy calculations

CASSCF and CASPT2 single point calculations have been carried out on top of the B-P optimized geometries for singlet and triplet states (see Sec. 2). Basis I (Mn ANO-rcc [63, 64] contracted to [7s6p5d2f1g]; N, C, O, S, Cl ANO-s [65] contracted to [4s3p1d]; H ANO-s contracted to [2s]) and Basis II (ANO-rcc on all atoms contracted to [7s6p5d3f2g1h] for Mn, [4s3p2d1f] for N, C, O, S, Cl and [3s1p] for H) have been compared. The [10,12] active space consists of the Mn 3d orbitals ($3d_{xz}$, $3d_{yz}$, $3d_{xy}$, $3d_{x^2-y^2}$ and $3d_{z^2}$), three diffuse orbitals that account for the double shell effect ($4d_{xz}$, $4d_{yz}$ and $4d_{xy}$), and four ligand orbitals ($2p_x$, $2p_y$ and $2p_z$ for N_{axial} and σ for $N_{pyrrole}$). This active space is required to obtain an accurate reference wave functions [66]. Instead of being localized, the Mn 3d and ligand orbitals form bonding and anti-bonding combinations. The orientation of the system with the $N_{pyrrole}$ on the x - and y -axes makes that Mn $3d_{xz}$, $3d_{yz}$ and $3d_{z^2}$ interact with N_{axial} $2p_x$, $2p_y$ and $2p_z$ orbitals to form a bonding and anti-bonding pair of orbitals with occupations close to 2 and 0 respectively. Mn $3d_{x^2-y^2}$ combines with $N_{pyrrole}$ $2p_x$ and $2p_y$ to form σ and σ^* orbitals. Mn $3d_{xy}$ is non-bonding and more stable than the anti-bonding combinations. Results of [10,12]-CASPT2 calculations are summarized in Table 2.

Table 2: [10,12]-CASPT2 main configurations and relative energies (in eV) of the singlet and triplet states obtained with the B-P/TZVP optimized geometries.

		[10,12]-CASPT2	
	main configuration	Basis I	Basis II
Mn(Cor)(NMes)			
S=0	$(3d_{xy})^2$	0.00	0.00
S=1	$(3d_{xy})^1(3d_{xz} - 2p_x)^{*1}$	0.17	0.18
	$(3d_{xy})^1(3d_{yz} - 2p_y)^{*1}$	1.19	1.18
Mn(Cz)(NMes)			
S=0	$(3d_{xy})^2$	0.00	0.00
S=1	$(3d_{xy})^1(3d_{xz} - 2p_x)^{*1}$	0.24	0.25
	$(3d_{xy})^1(3d_{yz} - 2p_y)^{*1}$	1.19	1.19
Mn(Cor)(NtClPh)			
S=0	$(3d_{xy})^2$	0.00	0.00
S=1	$(3d_{xy})^1(3d_{xz} - 2p_x)^{*1}$	0.16	0.17
	$(3d_{xy})^1(3d_{yz} - 2p_y)^{*1}$	0.85	0.87
Mn(Cor)(NTs)			
S=0	$(3d_{xy})^2$	0.00	0.00
S=1	$(3d_{xy})^1(3d_{yz} - 2p_y)^{*1}$	-0.02	0.00

CASPT2 results predict singlet ground states for all complexes except for the NTs complex with the weakest π -donating axial ligand for which both spin states are predicted to be nearly degenerate. The second triplet state of the complex with the Nt-ClPh ligand, which is of intermediate π -donating strength, has a lower relative energy than the second triplet state in the NMes complex, which has the strongest π -donating ligand. This shows that the stronger electron-donation increases the $3d_{xz,yz}$ relative orbital energies. A considerable energy gap separates the first and second triplets of all imido-complexes contrasting with complexes with the cylindrically symmetric oxo axial ligands, for which the two high-spin states are degenerate [32].

The Mn-N_{axial}-R angle of the triplet state geometries is not linear, diminishing the overlap of the ($3d_{xz}$ - $2p_x$) or the ($3d_{yz}$ - $2p_y$) pair of orbitals. Taking as example the

NTs complex in the triplet state (see Fig.7), the axial ligand is bend towards the y axis and the mixing between $3d_{yz}$ and $2p_y$ is smaller than between $3d_{xz}$ and $2p_x$. As a consequence, the anti-bonding ($3d_{yz}\text{-}2p_y$)^{*} orbital is stabilized and its occupation is favoured [50]. When compared to corrole, the smaller cavity size of corrolazine results in a shortening of the Mn-N_{pyrrole} bond and an increase of Δ , giving rise to an even more unstable triplet state. The energy of the triplet state of Mn(Cor)(NTs) is found at a much lower energy with CASPT2 than with B-P, but the description is still not consistent with the experimental data.

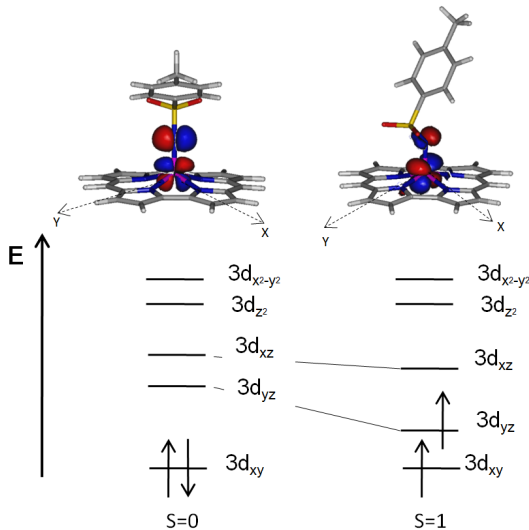


Figure 7: Schematic representation of the energetic ordering of the molecular orbitals for the alternated singlet (*left*) and eclipsed first triplet (*right*) states of Mn(Cor)(NTs) (isocontour=0.05).

3.2 Reoptimization of Mn(Cor)(NTs)

The near-degeneracy of the singlet and lowest triplet state of the NTs complex triggers the need to reconsider the geometry optimization performed with the B-P functional. In many cases reoptimization of some key geometrical parameters with CASPT2 can lead to important improvements in the relative energies of interest [67]. In this case the most obvious parameters to be reoptimized are the Mn-N distance and the Mn-N-S angle. The alternated and eclipsed conformations (see Fig.4) have been taken as

starting point for the singlet and triplet states, respectively, for a [10,12]-CASPT2 scan along the axial coordination distance. At each point of the scan, the Mn-N_{axial} distance and the Mn-N-S angle were kept fixed at a certain value while the rest of structural parameters was optimized with B-P/TZVP. CASPT2 single point calculations with Basis I have been performed to evaluate the energy of the so-obtained geometries. Since the axial coordination angle is linear in the singlet geometry, the angle was only scanned for the triplet state.

As can be seen in Table 3, [10,12]-CASPT2 calculations with Basis I and Basis II predict the experimentally expected high-spin ground state and a reasonable gap with the singlet state. Comparison of the [10,12]-CASPT2/B-P geometries with those reported in Sec. 2 reveals that small variations in the Mn-N_{axial} distance (on the order of 0.03 Å) and the Mn–N_{axial}–S angle ($\sim 10^\circ$) can remove the degeneracy of the S=0 and S=1 states of these complexes. At difference with the other imido-complexes, NTs contains a tetrahedral sulphur atom between N_{axial} and the phenyl ring (see Fig. 3), giving flexibility to the structure of the axial ligand and favouring geometries with a non-linear coordination angle. In conclusion, being the weaker π -donating ligand and favouring bent axial angles, NTs accomplishes all the factors to exhibit a triplet ground state.

Table 3: Main electronic configurations, reoptimized Mn–N_{axial} distances (in Å) and Mn–N_{axial}–S angles (in degrees), and relative energies (in eV) of the alternated (S=0) and eclipsed (S=1) states of the NTs imido-complex. B-P results of Sec. 2 in parenthesis for comparison.

	CASPT2			
	Mn-N _{axial}	Mn-N _{axial} –S	Basis I	Basis II
alternated				
(3d _{xy}) ²	1.60 (1.62)	168.2 (167.0)	0.00	0.00
eclipsed				
(3d _{xy}) ¹ (3d _{yz} – 2p _y) [*] ¹	1.75 (1.71)	125.0 (132.0)	-0.08	-0.07

3.3 Core correlation: a CASPT2 and DDCI comparison

The addition by perturbative methods of the electron correlation that is not taken into account in the CASSCF approach leads to important changes of the relative energy of the spin states in the here-studied imido-complexes and brings the theoretical estimates in good agreement with experimental data. Being of moderate computational cost, CASPT2 seems to be a very efficient computational strategy to obtain accurate relative energies of spin states. The validity of applying a level shift of 0.1 Eh to avoid the appearance of intruder states and the choice of the zeroth-order Hamiltonian with IPEA equal to 0.25 is well-established and the only point that deserves further attention is the accuracy of the perturbative estimate of the core correlation. Typically, the core electrons of main group elements are excluded from the CASPT2 energy estimation, since they do not introduce any differential effect on the energies of spin states. In the case of first-row transition metals, the situation is slightly different because the semi-core 3s-3p electrons can change the relative energy of the spin states by \sim 0.1–0.2 eV when included in the multireferential second-order perturbative correction [68]. However, recent results by Pierloot et al. [69] indicate that the correlation energy description by CASPT2 of these electrons is probably not fully consistent leading to wrong estimations of the high and low-spin energies in some cases.

In order to validate the multiconfigurational calculations of the present work, the Mn 3s-3p CASPT2 electron correlation in all the imido-complexes has been compared with a variational estimate obtained by DDCI [70, 71]. As can be seen in Table 4, the CASPT2 3s-3p contribution is quantitatively similar for all complexes and in all cases stabilizes the triplet state by around 0.2 eV. The importance of 3s-3p correlation is reflected in the fact that it inverts the ground state of Mn(Cor)(NTs). To make feasible the DDCI calculations a significant reduction of the molecular orbital space is required. The doubly occupied and empty CASSCF orbitals have been localized following the scheme outlined in Ref. [72–74], and subsequently, classified in terms of core, σ and π orbitals to select the most relevant orbitals to be taken into account in the DDCI calculation. Two molecular orbital spaces were considered, the first contains the π and π^* orbitals in addition to the twelve active orbitals, the second space extends the first one with the Mn 3s-3p orbitals. The reference wave function for the DDCI

calculation is constructed from a [2,2]-CASCI calculation using the orbitals that are singly occupied in the triplet state; $3d_{xy}$ and $(3d_{xz}-2p_x)^*$ or $(3d_{yz}-2p_y)^*$ depending on the complex. The [2,2]-DDCI estimate of the 3s-3p correlation contributions to the triplet-singlet energy difference are slightly lower than those calculated with [10,12]-CASPT2 but no relevant differences are detected. The addition of more virtual orbitals in the DDCI calculation increases the correlation energy, but has no differential effects.

Table 4: [10,12]-CASPT2 and [2,2]-DDCI estimates of the Mn 3s-3p electron correlation contribution (in eV) to the triplet-singlet energy difference for the four imido-complexes.

	[10,12]-CASPT2	[2,2]-DDCI
Mn(Cor)(NMes)	-0.24	-0.13
Mn(Cz)(NMes)	-0.25	-0.17
Mn(Cor)(NtClIPh)	-0.11	-0.13
Mn(Cor)(NTs)	-0.21	-0.11

3.4 Wave function analysis

The assignment of charges to atoms (or groups of atoms) in a molecule is a delicate matter. The atomic charge is not observable and computationally derived charges show a large dependence on the strategy applied to calculate them. Without pretending to determine *exact* charges, we have used an orthogonal valence bond reading of the multiconfigurational wave function to extract more information about the electronic structure and assign populations to the Mn atom in the different complexes. Atomic-like orbitals are ideally suited to describe many chemical concepts in terms of the valence bond theory in an intuitive manner [75], but they are computationally speaking not the most ideal choice as orbital basis. On the other hand, CASSCF wave functions are normally expressed with molecular orbitals, computationally much simpler to handle and also because they give direct information about molecular spectroscopy and ionization potentials, among other properties [76]. Yet the transformation of these delocalized orbitals to atomic-like orbitals and the subsequent re-expression of the multiconfigurational CASSCF wave function in this new orbital basis makes pos-

sible to capture the electronic structure in similar intuitive concepts as in traditional valence bond calculations [77]. An example of orbital localization is illustrated in Fig. 8. The localization procedure transfers the covalency contained in the delocalized orbitals to the configuration expansion [78, 79]. In the present case all twelve orbitals of the active space have been localized using the same localization procedure as in the previous section.

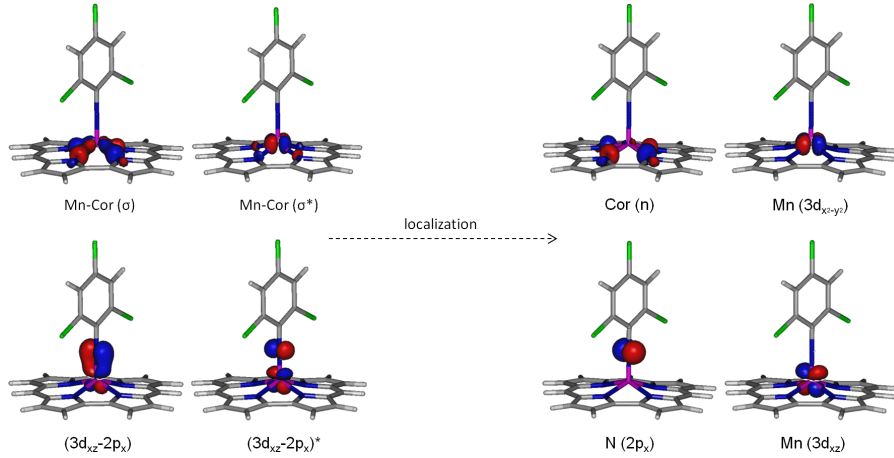


Figure 8: Example of orbitals before and after the localization procedure (isocontour=0.05). σ and $(3d_{xz}-2p_x)$ bonding and anti-bonding couple of orbitals are transformed in metal, imide and corrole localized orbitals.

Table 5 summarizes the orthogonal valence bond analysis of the electronic structure of the four imido-complexes. For this purpose, the configurations of the CASSCF wave function have been classified by the number of electrons in the metal valence orbitals and the weight of the configurations has been summed for each subgroup, as shown in Table 5. The wave function is dominated by configurations with 5 electrons on the Mn ion, but configurations with 4 or 6 electrons also contribute significantly. The weighted sum of the d -electrons in each configuration gives what we call the d -count, which is close to 5 in all complexes. In a purely ionic model with a trianionic corrole and a dianionic imide ligand, one would rather expect a d -count of 2, corresponding to Mn^V . In the present analysis the effective charge differs from the formal charge and indicates that there is an important charge transfer from the coordination sphere to the Mn ion, which is probably better considered as an effective Mn^{2+} ion.

Table 5: Orthogonal valence bond analysis of the [10,12]-CASSCF wave function of the four imido-complexes. Electronic configurations in the wave function are grouped by the number of electrons in the Mn d-orbitals and the total weight is given as a percentage. The d-count is the weighted sum of electrons on the metal centre.

	Mn						
	7e ⁻	6e ⁻	5e ⁻	4e ⁻	3e ⁻	total weight	d-count
Mn(Cor)(NMes)	4.9	23.5	42.6	24.8	3.0	98.7	5.03
Mn(Cz)(NMes)	5.0	23.6	42.1	24.9	3.2	98.9	5.02
Mn(Cor)(NtClPh)	5.3	24.2	42.3	24.0	2.9	98.7	5.05
Mn(Cor)(NTs)	6.2	25.9	41.3	21.7	2.4	97.5	5.12

The electron count of the coordination sphere around the metal centre can be treated in a similar way as the assignment of the Mn charge. In the present calculations, a standard two-electron dative bond from the trianionic corrole to Mn is represented with 2 electrons in the corrole or corrulazine σ active orbital. As can be seen in Table 6, only half of the configurations corresponds to this situation. The other half has only one electron in the corrole or corrulazine σ -orbital. This corresponds to a strongly covalent Mn $3d_{x^2-y^2}-\sigma$ bond. The present imido-Mn complexes are therefore not completely trianionic. With the same analysis the imido-to-metal charge transfer can be quantified by looking at the occupation of the three $2p_x$, $2p_y$ and $2p_z$ active orbitals localized on the nitrogen atom. The fact that the electron count of these is close to 3.5 in all cases denotes that N-R group transfers 2.5 electrons to the d orbitals of the metal centre. To sum up, the transfer of nearly 3 electrons (0.5 from corrole and 2.5 from imide) from the coordination sphere to the metal centre is the key to understand how TMs are stabilized in these imido-complexes [29, 80–82].

Table 6: Orthogonal valence bond analysis of the [10,12]-CASSCF wave function of the four imido-complexes. Electronic configurations in the wave function are grouped by the number of electrons in the corrole, corrolazine and imide ligands and the total weight is given as percentage.

	Cor/Cz				NR			
	$2e^-$	$1e^-$	Count	$5e^-$	$4e^-$	$3e^-$	$2e^-$	Count
Mn(Cor)(NMes)	47.0	45.6	1.41	9.0	44.3	38.0	7.3	3.56
Mn(Cz)(NMes)	44.8	47.2	1.38	9.8	45.2	37.0	6.7	3.59
Mn(Cor)(NtClPh)	46.0	46.3	1.39	9.4	43.1	37.8	8.2	3.55
Mn(Cor)(NTs)	45.5	45.7	1.39	8.5	39.6	39.2	10.0	3.48

4 Conclusions

The computational study presented here shows that the axial N-R ligand plays a fundamental role in the relative stability of the electronic states with different spin moment. The combination of DFT geometry optimizations and CASPT2 single-point calculations results in a description of the relative energies of the singlet and triplet coupled states that is consistent with the experimental information on four different imido-Mn corrole and corrolazine complexes. The DFT optimized geometries show identical corrole and corrolazine coordination distances in singlet and triplet, but important variations are observed in the coordination of the axial ligand. The singlet presents short distances and linear coordination, while the bond distance is longer for the triplet coupling and the axial ligand also has a marked tendency to coordinate in a bend fashion. Furthermore, it is observed that electron withdrawing groups in the axial ligand reduce the π interaction between metal and ligand and reduce the gap between the two singly occupied orbitals of the triplet state, and hence, stabilizing it with respect to the singlet state. Hence, it is not unexpected that the system with the strongest electron withdrawing group, the NTs complex, has a triplet ground state.

The orthogonal valence bond reading of the wave functions reveals important electron charge transfers from both the corrole/corrolazine ligand and the axial ligands to

the Mn. The formal charge of Mn within an ionic model of the complexes corresponds to Mn⁵⁺. However, the wave function shows that this high charge is reduced to an effective charge of 2+ by a transfer of nearly three electrons (2.5 from the axial ligand and 0.5 from the corrole/corrolazine) to the metal centre.

Acknowledgments

Financial support has been provided by the Spanish Administration (Project CTQ2014-51938-P), the Generalitat de Catalunya (Projects 2014SGR199 and Xarxa d'R+D+I en Química Teòrica i Computacional, XRQTC) and the European Union (COST Action ECOSTBio CM1305). The Flemish Science Foundation (FWO) is acknowledged for financial support. Computational resources and services used in this work were provided by the VSC (Flemish Supercomputer Center), funded by the Hercules Foundation and the Flemish Government – department EWI.

References

- [1] R. Weiss, V. Bulach, A. Gold, J. Terner, and A. Trautwein, *J. Biol. Inorg. Chem.* **6**, 831 (2001).
- [2] J. Groves, *J. Inorg. Biochem.* **100**, 434 (2006).
- [3] W. Nam, *Acc. Chem. Res.* **40**, 522 (2007).
- [4] H. Chen, J. Song, W. Lai, W. Wu, and S. Shaik, *J. Chem. Theory Comput.* **6**, 940 (2010).
- [5] J. Rittle and M. Green, *Science* **330**, 933 (2010).
- [6] I. Viciana, R. Castillo, and S. Marti, *J. Comput. Chem.* **36**, 1736 (2015).
- [7] J. Groves, W. Kruper, and R. Haushalter, *J. Am. Chem. Soc.* **102**, 6375 (1980).
- [8] R. Breslow and S. Gellman, *J. Chem. Soc., Chem. Commun.* pp. 1400–1401 (1982).
- [9] R. Breslow and S. Gellman, *J. Am. Chem. Soc.* **105**, 6728 (1983).
- [10] J. Groves and T. Takahashi, *J. Am. Chem. Soc.* **105**, 2073 (1983).

- [11] E. Svastits, J. Dawson, R. Breslow, and S. Gellman, *J. Ame. Chem. Soc.* **107**, 6427 (1985).
- [12] N. Jin, J. Bourassa, S. Tizio, and J. Groves, *Angew. Chem. Int. Ed.* **39**, 3849 (2000).
- [13] N. Jin, M. Ibrahim, T. Spiro, and J. Groves, *J. Am. Chem. Soc.* **129**, 12416 (2007).
- [14] W. Song, M. Seo, S. George, T. Ohta, R. Song, M. Kang, T. Tosha, T. Kitagawa, E. Solomon, and W. Nam, *J. Am. Chem. Soc.* **129**, 1268 (2007).
- [15] S. Shaik, D. Danovich, A. Fiedler, D. Schroder, and H. Schwarz, *J. Am. Chem. Soc.* **129**, 1268 (1995).
- [16] J. Detrich, O. Reinaud, A. Rheingold, and K. Theopold, *J. Am. Chem. Soc.* **117**, 11745 (1995).
- [17] D. Schroder, S. Shaik, and H. Schwarz, *Acc. Chem. Res.* **33**, 139 (2000).
- [18] N. Jin and J. Groves, *J. Am. Chem. Soc.* **121**, 2923 (1999).
- [19] F. De Angelis, N. Jin, R. Car, and J. Groves, *Inorg. Chem.* **45**, 4268 (2006).
- [20] R. Latifi, L. Tahsini, B. Karamzadeh, N. Safari, W. Nam, and S. de Visser, *Arch. Biochem. Biophys.* **507**, 4 (2011).
- [21] A. Jasat and D. Dolphin, *Chem. Rev.* **97**, 2267 (1997).
- [22] R. Paolesse, S. Nardis, F. Sagone, and R. Khoury, *J. Org. Chem.* **66**, 550 (2001).
- [23] A. Johnson and I. Kay, *Proc. Chem. Soc.* p. 89 (1964).
- [24] Z. Gross, N. Galili, and I. Saltsman, *Angew. Chem. Int. Ed.* **38**, 1427 (1999).
- [25] Z. Gross, N. Galili, L. Simkhovich, I. Saltsman, M. Botoshansky, D. Blaser, R. Boese, and I. Goldberg, *Org. Lett.* **1**, 599 (1999).
- [26] Z. Gross, *J. Biol. Inorg. Chem.* **6**, 733 (2001).
- [27] I. Aviv and Z. Gross, *Chem. Commun.* pp. 1987–1999 (2007).

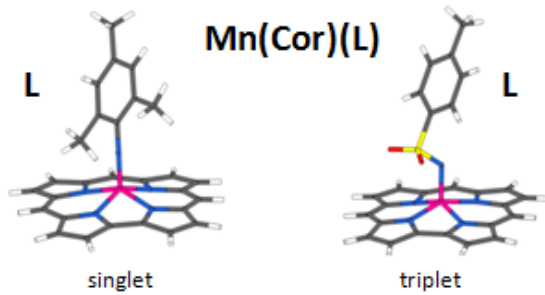
- [28] I. Aviv and Z. Gross, *Chem. Eur. J.* **15**, 8382 (2009).
- [29] K. Pierloot, H. Zhao, and S. Vancoillie, *Inorg. Chem.* **49**, 10316 (2010).
- [30] S. Berg, K. Thomas, C. Beavers, and A. Ghosh, *Inorg. Chem.* **51**, 9911 (2012).
- [31] K. Thomas, A. Alemayehu, J. Conradie, C. Beavers, and A. Ghosh, *Acc. Chem. Res.* **45**, 1203 (2012).
- [32] H. Zhao, K. Pierloot, E. Langner, J. Swarts, J. Conradie, and A. Ghosh, *Inorg. Chem.* **51**, 4002 (2012).
- [33] A. Alemayehu, K. Gagnon, J. Terner, and A. Ghosh, *Angew. Chem. Int. Ed.* **53**, 14411 (2014).
- [34] J. Capar, J. Conradie, C. Beavers, and A. Ghosh, *J. Phys. Chem. A* **119**, 3452 (2015).
- [35] B. Ramdhanie, C. Stern, and D. Goldberg, *J. Am. Chem. Soc.* **123**, 9447 (2001).
- [36] W. Kerber and D. Goldberg, *J. Inorg. Biochem.* **100**, 838 (2006).
- [37] D. P. Goldberg, *Acc. Chem. Res.* **40**, 626 (2007).
- [38] E. Tangen and A. Ghosh, *J. Am. Chem. Soc.* **124**, 8117 (2002).
- [39] H. Liu, M. Mahmood, S. Qiu, and C. Chang, *Coord. Chem. Rev.* **257**, 1306 (2013).
- [40] Z. Gross, G. Golubkov, and L. Simkhovich, *Angew. Chem. Int. Ed.* **39**, 4045 (2000).
- [41] H. Liu, T. Lai, L. Yeung, and C. Chang, *Org. Lett.* **5**, 617 (2003).
- [42] Z. Gross and H. Gray, *Adv. Synth. Catal.* **346**, 165 (2004).
- [43] A. Kumar, I. Goldberg, M. Botoshansky, Y. Buchman, and Z. Gross, *J. Am. Chem. Soc.* **132**, 15233 (2010).
- [44] B. Mandimutsira, B. Ramdhanie, R. Todd, H. Wang, A. Zareba, R. Czemuzevicz, and D. Goldberg, *J. Am. Chem. Soc.* **124**, 15170 (2002).

- [45] D. Lansky, B. Mandimutsira, B. Ramdhanie, M. Clausen, J. Penner-Hahn, S. Zvyagin, J. Telser, J. Krzystek, R. Zhan, Z. Ou, et al., Inorg. Chem. **44**, 4485 (2005).
- [46] D. Lansky and D. Goldberg, Inorg. Chem. **45**, 5119 (2006).
- [47] R. A. Eikey, S. I. Khan, and M. M. Abu-Omar, Angew. Chem. Int. Ed. **41**, 3592 (2002).
- [48] N. Edwards, R. Eikey, M. Loring, and M. Abu-Omar, Inorg. Chem. **44**, 3700 (2005).
- [49] D. E. Lansky, J. R. Kosack, A. A. N. Sarjeant, and D. P. Goldberg, Inorg. Chem. **45**, 8477 (2006).
- [50] M. J. Zdilla and M. M. Abu-Omar, J. Am. Chem. Soc. **128**, 16971 (2006).
- [51] M. Abu-Omar, Dalton Trans. **40**, 3435 (2011).
- [52] F. Weigend, M. Haser, H. Patzelt, and R. Ahlrichs, Chem. Phys. Lett. **294**, 143 (1998).
- [53] F. Weigend and R. Ahlrichs, Phys. Chem. Chem. Phys. **7**, 3297 (2005).
- [54] J. Perdew and Y. Wang, Phys. Rev. B **45**, 13244 (1992).
- [55] J. Perdew, K. Burke, and M. Ernzerhof, Phys. Rev. Lett. **77**, 3865 (1996).
- [56] J. Perdew, M. Ernzerhof, and K. Burke, J. Chem. Phys. **105**, 9982 (1996).
- [57] J. Perdew, Phys. Rev. B **33**, 8822 (1986).
- [58] A. Becke, Phys. Rev. A **38**, 3098 (1988).
- [59] S. De Visser, F. Ogliaro, Z. Gross, and S. Shaik, Chem. Eur. J. **7**, 4954 (2001).
- [60] A. Ghosh and P. Taylor, Current Opinion in Chemical Biology **7**, 113 (2003).
- [61] M. Swart, A. Groenhof, A. Ehlers, and K. Lammertsma, J. Phys. Chem. A **108**, 5479 (2004).
- [62] H. Chen, W. Lai, and S. Shaik, J. Phys. Chem. B **115**, 1727 (2011).

- [63] B. Roos, R. Lindh, P.-. Malmqvist, V. Veryazov, and P.-O. Widmark, *J. Phys. Chem. A* **108**, 2851 (2004).
- [64] B. Roos, R. Lindh, P.-. Malmqvist, V. Veryazov, and P.-O. Widmark, *J. Phys. Chem. A* **109**, 6575 (2005).
- [65] K. Pierloot, B. Dumez, P.-O. Widmark, and B. Roos, *Theor. Chim. Acta* **90**, 87 (1995).
- [66] K. Pierloot, *Int. J. Quantum Chem.* **111**, 3291 (2011).
- [67] K. Pierloot and S. Vancoillie, *J. Chem. Phys.* **125**, 124303 (2006).
- [68] K. Pierloot, E. Tsokos, and B. Roos, *Chem. Phys. Lett.* **214**, 583 (1993).
- [69] (To be published).
- [70] J. Miralles, J. Daudey, and R. Caballol, *Chem. Phys. Lett.* **198**, 555 (1992).
- [71] J. Miralles, O. Castell, R. Caballol, and J. Malrieu, *J. Chem. Phys.* **172**, 33 (1993).
- [72] D. Maynau, S. Evangelisti, N. Guihery, C. Calzado, and J. Malrieu, *J. Chem. Phys.* **116**, 10060 (2002).
- [73] C. Calzado, S. Evangelisti, and D. Maynau, *J. Phys. Chem. A* **107**, 7581 (2003).
- [74] N. Ben Amor, F. Bessac, S. Hoyau, and D. Maynau, *J. Chem. Phys.* **135** (2011).
- [75] S. Shaik and P. Hiberty, *A Chemist's Guide to Valence Bond Theory* (Wiley, 2007), ISBN 9780470192580.
- [76] C. Angeli, R. Cimiraglia, and J.-P. Malrieu, *J. Chem. Educ.* **85**, 150 (2008).
- [77] W. Wu, P. Su, S. Shaik, and P. Hiberty, *Phys. Chem. Chem. Phys.* **111**, 7557 (2011).
- [78] A. Sadoc, R. Broer, and C. de Graaf, *J. Chem. Phys.* **126**, 134709 (2007).
- [79] A. Sadoc, R. Broer, and C. de Graaf, *Chem. Phys. Lett.* **454**, 196 (2008).

- [80] J. Zapata-Rivera, R. Caballol, and C. Calzado, *Phys. Chem. Chem. Phys.* **13**, 20241 (2011).
- [81] J. Zapata-Rivera, R. Caballol, and C. Calzado, *J. Comput. Chem.* **32**, 1144 (2011).
- [82] J. Zapata-Rivera, R. Caballol, and C. Calzado, *J. Comput. Chem.* **33**, 1407 (2012).

For Table of Contents Only



Synopsis

Multiconfigurational perturbation theory energy calculations on DFT optimized geometries of four Mn corrole and corrolazine are reported to clarify the role of the axial imide ligand on the relative stability of the low-lying magnetic states of these complexes. The analysis of the multiconfigurational wave function provides insights of how both equatorial corrole/corrolazine and axial imide ligands stabilize the formally Mn^{V} ion.